

## 3D-localization of the $\alpha$ -subunit of $F_0F_1$ -ATP synthase by time resolved single-molecule FRET

Monika G. Düser<sup>a</sup>, Nawid Zarrabi<sup>a</sup>, Yumin Bi<sup>b</sup>, Boris Zimmermann<sup>c</sup>, Stanley D. Dunn<sup>b</sup>, Michael Börsch<sup>\*a</sup>

<sup>a</sup> 3. Physikalisches Institut, Universität Stuttgart, Pfaffenwaldring 57, 70569 Stuttgart, Germany

<sup>b</sup> Department of Biochemistry, University of Western Ontario, London, Ontario, Canada, N6A5C1

<sup>c</sup> Institut für Physikalische Chemie, Albert-Ludwig-Universität Freiburg, Albertstr.23 a, 79104 Freiburg, Germany

### ABSTRACT

$F_0F_1$ -ATP synthases catalyze the ATP formation from ADP and phosphate in the membranes of mitochondria, chloroplasts and bacteria. Internal rotation of subunits couples the chemical reaction at the  $F_1$  part to the proton translocation through the  $F_0$  part. In these enzymes, the membrane-embedded  $\alpha$ -subunit is part of the non-rotating 'stator' subunits and provides the proton channel of the  $F_0$  motor. At present, the relative position of the  $\alpha$ -subunit is not known. We examined the rotary movements of the  $\varepsilon$ -subunit with respect to the non-rotating  $\alpha$ -subunit by time resolved single-molecule fluorescence resonance energy transfer (FRET) using a novel pulsed laser diode. Rotation of the  $\varepsilon$ -subunit during ATP hydrolysis was divided into three major steps. The stopping positions of  $\varepsilon$  resulted in three distinct FRET efficiency levels and FRET donor lifetimes. From these FRET efficiencies the position of the FRET donor at the  $\alpha$ -subunit was calculated. Different populations of the three resting positions of  $\varepsilon$ , which were observed previously, enabled us to scrutinize the models for the position of the  $\alpha$ -subunit in the  $F_0$  part.

Keywords: single-molecule, ATP synthase, fluorescence resonance energy transfer

### INTRODUCTION

$F_0F_1$ -ATP synthases are the membrane-embedded enzymes in mitochondria, chloroplasts and bacteria that supply the cells with the 'universal chemical energy currency' adenosine triphosphate, ATP. These multi subunit enzymes have a bipartite structure. Catalysis of ATP formation from ADP and phosphate is driven by an electrochemical potential difference of ions across the plasma membrane, for instance by a difference in proton concentration in case of the bacterium *Escherichia coli*. A rotary movement of the proton turbine-like ring of  $c$ -subunits of the  $F_0$  portion in the membrane is transduced to a three-stepped rotation of the central  $\gamma$ - and  $\varepsilon$ -subunit of the  $F_1$  portion, and this induces the conformational changes of the binding sites in the  $F_1$  part of the enzyme that catalyze the chemical reaction<sup>1-3</sup>.

The overall structure of the  $F_0F_1$ -ATP synthase has been visualized by electron microscopy<sup>4,5</sup>. Single particle analysis and three-dimensional image reconstruction revealed two connections between the  $F_1$  head piece outside the membrane and the  $F_0$  part as the foot piece embedded in the membrane. The central stalk of the *E. coli* enzyme consists of the subunits  $\gamma$  and  $\varepsilon$ , the peripheral connection is constituted by the  $b$ -subunit dimer. Structural details of  $F_0F_1$ -ATP synthase at atomic resolution cover the  $F_1$  part with the subunits  $\alpha_3\beta_3\gamma\delta\varepsilon$ <sup>6</sup>. Additional structural information was gathered using NMR spectroscopy and X-ray crystallography of isolated subunits.

---

\* m.boersch@physik.uni-stuttgart.de; phone 49 711 685 4632; fax 49 711 685 5281; www.m-boersch.org

The  $F_0$  part has a subunit composition  $ab_2c_n$  with  $n$  ranging from 10 to 15 depending on the organism. The structure of the  $c_{11}$ -ring from the  $\text{Na}^+$ -driven enzyme of *Ilyobacter tartaricus* has been solved recently at 2.4 Å resolution<sup>7</sup>. The adjacent  $a$ -subunit consists of five transmembrane helices and is thought to exhibit the transport channels for the ions or protons to the binding site on the  $c$ -subunit, but structural details of subunit  $a$  are not yet available<sup>8</sup>. Information for the N-terminal parts of the  $b$ -subunits connecting the membrane portion with the  $F_1$  headpiece was obtained by NMR, and the dimerization domain of the  $b$ -subunits has been crystallized. Taking this information together, a model for the *E. coli* enzyme can be derived and compared to the three-dimensional images of the enzyme obtained from electron microscopy.

However, the relative position of the  $a$ -subunit in the membrane with respect to the  $b$ -subunits remains unclear. Because the  $a$ -subunit is hydrophobic and mostly embedded in the lipid membrane, the detergent used to solubilize the  $F_0F_1$ -ATP synthase for electron microscopy imaging is still attached to the hydrophobic protein surfaces and hides the position of the  $a$ -subunit. In fact, the size of the  $c$ -ring as seen in the electron micrographs appears to be significantly larger than the 5 nm diameter found in the crystal structure<sup>4</sup>. To identify the position of the proton-conducting  $a$ -subunit of  $F_0$ , and to discriminate between a symmetric arrangement between the two  $b$ -subunits or an asymmetric arrangement on one side of the  $b$ -subunits, we employed a triangulation approach using a set of intramolecular distance measurements within a single ATP synthase.

We use Förster-type resonance energy transfer (FRET) as an appropriate method for distance measurements in the range of 2 to 8 nm<sup>9</sup>. It is based on non-radiative energy transfer between two fluorophores with a strong distance dependence<sup>10</sup>. Despite the general applicability, problems of ensemble averaging limit the FRET approach. The labeling degree for site-specific attachment of reactive fluorophores to the different amino acids is not 100 percent and, as a result, the labeled protein ensemble contains always more than one fluorescent species that are difficult to separate. Multiple conformations of a protein and conformational fluctuations during the measurement time require a resolution of more than one distance simultaneously. To overcome these limitations, a structure determination approach has been developed that is based on analyzing only a single molecule at a given time interval. Single-molecule FRET measurements have been introduced about one decade ago and the method has matured to a standard fluorescence technique in many laboratories. Here we report on time resolved single-molecule FRET experiments and describe the recent progress we made towards a non-biased intramolecular distance determination.

## METHODOLOGY

### 1. Preparation of the single FRET-labeled $F_0F_1$ -ATP synthase in a single liposome

#### 1.1. EGFP as the FRET donor fused to the $a$ -subunit of $F_0$

We have permanently fused a fluorescent probe to the  $a$ -subunit of the  $F_0$  part of ATP synthase from *Escherichia coli*. The fusion with 'enhanced Green Fluorescent Protein', EGFP (Clontech) was genetically introduced to the C-terminus of the  $a$ -subunit with a spacer of four additional amino acids (details will be given elsewhere). EGFP was the FRET donor fluorophore in the single-molecule experiments. The *E. coli* cells grow at similar rates compared to the non-mutated bacterial strain. In confocal laser scanning images, only the membranes of the *E. coli* cells were fluorescent while the cytoplasm appeared dark. The  $F_0F_1$ -ATP synthases were isolated from the membranes as described<sup>11</sup>. The purified enzymes were reconstituted substoichiometrically into pre-formed lipid vesicles, liposomes, of approximately 100 nm in diameter<sup>12</sup> to yield not more than a single  $F_0F_1$  per liposome.

#### 1.2. Alexa-568 as the FRET acceptor bound to the $\epsilon$ -subunit of $F_1$

The FRET acceptor was covalently bound to a cysteine residue in the  $\epsilon$ -subunit of the  $F_1$  part. This cysteine has been used for recent single-molecule FRET experiments<sup>11</sup>. The amino acid position 56 of the  $\epsilon$ -subunit for introducing this cysteine mutation was chosen for two reasons. At first, it is located on the surface of the subunit to be accessible for the chemical reaction with the Alexa-568-maleimide. In the ATP synthase used for labeling, other cysteine residues were present, and, therefore, a specific labeling of  $\epsilon 56$  was achievable for this buffer-exposed cysteine when it was reacted with maleimides within 4 minutes incubation time at 4° C. Secondly, the position of  $\epsilon 56$  was chosen as an optimized 'off

axis position', that is, located far away from the assumed axis of rotation for the central stalk of subunits  $\gamma$  and  $\epsilon$  of the  $F_1$  portion. The 'off axis position' of  $\epsilon 56$  ensured maximum distance changes to the EGFP at the static  $\alpha$ -subunit during rotation of the  $\epsilon$ -subunit under catalytic conditions. Accordingly, the transient changes in FRET efficiency between the fluorophores at the  $\alpha$ -subunit and the  $\epsilon$ -subunit were expected to be as large as possible.

### 1.3. Reassembling labeled $F_0$ and $F_1$ to yield a single functional $F_0F_1$ -ATP synthase in a single liposome

After separate labeling of the  $F_0$  part and the  $F_1$  part, a fully functional enzyme is obtained by the established reassembling procedures<sup>11,12</sup>. The  $F_0F_1$ -ATP synthase with the EGFP fusion to the  $\alpha$ -subunit was embedded into liposomes and  $Mg^{2+}$  ions were removed by buffer exchange. The  $Mg^{2+}$  concentration in the buffer was further reduced by complexation with EDTA. This caused the  $F_1$  parts to dissociate from the  $F_0$  parts. As the  $F_0$  parts remained in the liposomes, they can be separated by ultracentrifugation steps. In the next step, the fluorescently labeled  $F_1$  parts were added to the  $F_0$ , and reassembling occurred in the presence of  $Mg^{2+}$ . The binding constant for  $F_1$  to  $F_0$  in the presence of  $Mg^{2+}$  has been determined by this procedure in a FRET titration experiment using single-molecule counting<sup>13</sup>. After the reassembling, the functionality of the  $F_0F_1$ -ATP synthase in liposomes was probed by measuring the catalytic rates for ATP hydrolysis and ATP synthesis.

## 2. Confocal Setup for single-molecule FRET measurements

The single-molecule FRET experiments were done in a confocal microscope of local design based on a Olympus IX71 inverted microscope stage as described<sup>14</sup>. Briefly, for continuous-wave experiments excitation at 488 nm was provided by a fiber-coupled argon ion laser (Model 2020, Spectra Physics). The respective laser beam was expanded to approximately 3 mm diameter and coupled into a water immersion objective (UAPO 340, N.A. 1.15, Olympus) in epi-fluorescence configuration. Therefore, a dichroic beamsplitter (c488RDC, AHF Tübingen, Germany) was used. The laser focus was placed into 30-50  $\mu$ l droplets of buffer containing the ATP synthase and approximately 100  $\mu$ m away from the surface of the glass cover slide. Fluorescence was collected after passing the beamsplitter and the 100  $\mu$ m pinhole, and divided into two spectral ranges, one for the EGFP as the FRET donor, and the second for the Alexa-568 fluorophore as the FRET acceptor. EGFP fluorescence was detected by a single photon counting avalanche photodiode (SPCM-AQR 14, Perkin Elmer) between 498 nm and 567 nm (interference filter HQ532/70, AHF Tübingen). Alexa-568 fluorescence was detected after passing the dichroic mirror HQ 575 and a longpass filter LP 595 HQ (AHF Tübingen) by an avalanche photodiode SPCM-AQR 14 (Perkin Elmer). The third detection channel was not in use in these experiments. Signals were counted by a TCSPC card (SPC 630, Becker&Hickl, Berlin, Germany) with an 8-channel router electronics. For cw-excitation, a 44.9 MHz TTL sync signal was generated and inverted by a passive converter SIA 300 (Picoquant, Berlin, Germany) to trigger the TCSPC card.

### 2.1. Pulsed excitation of the FRET donor at 490 nm with the PicoTA 490 laser

The lifetime measurements of a single EGFP required pulsed excitation with ps pulse lengths. An novel amplified and frequency-doubled diode laser PicoTA 490 kindly provided from Picoquant, Berlin, Germany. This laser delivers 60 ps pulses at 490 nm with up to 80 MHz repetition rate which perfectly matches the excitation conditions for EGFP with its short fluorescence lifetime of 2.8 ns. The mean power of the laser was 2.8 mW and the laser intensity and beam position remained stable for 48 h. The TTL synchronization output of the diode driver unit was converted with a LTT 100 adaptor (Picoquant) and fed into the TCSPC card. With the possibility of external synchronization using TTL pulses with up to 80 MHz repetition, the PicoTA 490 is an ideal laser system for advanced single-molecule FRET experiments using pulsed interleaved excitation. To achieve a perfect circular beam profile, the laser should be passed through a fiber. In our experiments, a slightly elliptic beam was tolerated as we were using a large confocal excitation and detection volume to achieve long observation times for the freely diffusing liposomes in buffer. The laser pulses were coupled into the confocal microscope using the filters mentioned above.

### 2.2. Probing the FRET acceptor at 561 nm with the Cobolt Jive laser

We investigated the photophysics of the FRET acceptor Alexa-568 in an independent experiment using the Cobolt Jive as a highly-stabilized solid state laser system (kindly provided by Cobolt, Sweden) which emits at 561 nm with up to 30 mW cw power. The laser beam was coupled into the water immersion objective by a dichroic beamsplitter HQ575 in the

epi-fluorescence filter cube of the microscope. An interference filter HQ610/75 (AHF Tübingen) was used to detect the Alexa-568 fluorescence and to reject scattered light and the Raman bands from water.

### 2.3. Data analysis with the software 'Burst-Analyzer'

The TCSPC data files are analyzed with a locally developed software 'Burst-Analyzer' that is written by Nawid Zarrabi. In the TCSPC data, each photon count is registered with a macro time (50 ns time resolution relative to the start of the experiment) and with a micro time (ps time resolution relative to a laser pulse or another synchronization signal with several MHz repetition rate). The software reads the TCSPC data from all short sub-files, uses the routing information to associate the photon counts with the different detection channels and displays the fluorescence intensity trajectories with selectable time windows (usually 1 ms binning interval). One task of the 'Burst-Analyzer' is the identification of a single fluorescent molecule or particle for subsequent analysis, like the FRET-labeled ATP synthase in a lipid vesicle which appears as a photon burst in the time trajectories. To identify photon bursts showing FRET between donor and acceptor fluorophores, the FRET efficiency  $E_{FRET} = I_A / (I_A + \gamma I_D)$  is calculated per binning interval using the background-corrected intensities of the acceptor channel,  $I_A$ , and the donor channel,  $I_D$ . A correction factor,  $\gamma$ , accounts for different quantum yields and detection efficiencies of the set-up. In addition, a constant cross-talk fraction from the donor signal in the acceptor channel is subtracted to compensate for the spectral overlap from the donor fluorophore with the band filter of the acceptor channel.

In a separate window, the micro time histograms are showing the fluorescence decay curves. The lifetime calculations from the fluorescence decays are based on a maximum likelihood estimator<sup>15</sup> using the measured instrument response function, IRF. When changes of the FRET efficiency within a single photon burst are found, the different FRET levels can be analyzed by the typical properties like mean intensity, donor lifetime or donor-acceptor distance from the FRET efficiency. In parallel, the intensity autocorrelation function for one channel (or one time window, that is, for a single photon burst, respectively) can be calculated and displayed in order to verify the number of fluorescent molecules in the detection volume.

#### 2.3.1. The burst search algorithm

The software enables the definition of bursts and FRET levels, and it proposes algorithms for determining bursts and FRET levels automatically. The burst search algorithm scans the time traces and determines the burst edges based on threshold values: (i) the minimum intensity,  $I_{min}$ , (ii) the edge intensity,  $I_{edge}$ , and (iii) dark periods of the burst,  $t_{off}$ . False-positive bursts are removed by thresholds for the mean minimum intensity,  $\langle I \rangle_{min}$ , mean maximum intensity,  $\langle I \rangle_{max}$ , and a minimum burst length,  $\langle t \rangle_{min}$ . Briefly, the algorithm consists of four steps:

- The time bins are compared by  $I_{min}$ . If the intensity of the time bin is higher than  $I_{min}$ , a new burst will be created.
- The burst will be expanded in both time directions until the intensity drops below  $I_{edge}$ .
- To avoid incorrect separation of bursts (due to intensity decrease by diffusion to the peripheral parts of the confocal volume or due to blinking of the fluorophore), the time bins around the edges are compared with  $I_{edge}$ . Is there a time bin in the range of  $t_{off}$  away from the edges with an intensity larger than  $I_{edge}$ , then the burst will be expanded accordingly and the algorithm goes back to step 2 to enlarge the burst further more.
- In the last step, the attributes of all identified bursts will be compared with the mean parameters  $\langle I \rangle_{min}$ ,  $\langle I \rangle_{max}$ , and  $\langle t \rangle_{min}$  to remove false bursts. Bursts with a too low mean intensity will be removed by  $\langle I \rangle_{min}$ , bursts caused by multiple fluorophores in the focus or other bright vesicles will be removed by  $\langle I \rangle_{max}$ , and single fluorescent impurities with too short diffusion time will be removed by  $t_{min}$ .

#### 2.3.2. Identification of states with constant FRET efficiency

The automatic determination of a single FRET state or of interchanging FRET levels, respectively, within one photon burst is also realized by thresholds for the minimum intensity,  $I_{min}$ , the minimum level length,  $t_{min}$ , the maximum deviation of the mean proximity factor,  $dP_{max}$ , with  $P = I_A / (I_A + I_D)$ , and the time interval to the next FRET level,  $t_{adjacent}$ . The following 5 steps are processed for each burst:

- The time trace with the proximity factor information is scanned forward. Whenever the difference between  $P(t_0)$  and  $P(t_0-1)$  at the time  $t_0$  is greater than  $dP_{max}$ , the end-edge of the current FRET level and the start-edge of a new FRET level is placed at this point.

- After scanning of the current burst is completed, the created levels will be further processed: every level, which does not exceed  $I_{min}$  with at least one intensity value will be removed. Too dark levels with fluctuating proximity factors are removed by this step.
- A mean proximity factor,  $\langle P \rangle$ , for all remaining levels is calculated. Adjacent levels within a time distance less than  $t_{adjacent}$  and a difference in their  $\langle P \rangle$  values less than  $dP_{max}$  will be combined into one level.
- The time length of all remaining levels must exceed  $t_{min}$ , otherwise they will be removed in this step.
- Step 3 is processed a second time to combine all remaining adjacent steps.

### 2.3.3. Automatic FRET level sequence analysis

The last part of the automatic analysis is a verifying process for the sequence of all FRET levels within their bursts. The enzymes are sorted out that are not hydrolyzing ATP continuously, and, therefore, are not rotating unidirectionally in one direction. The main purpose of this step is to narrow the distribution of the conformations of the active enzyme. To check the sequence of levels within a burst, the mean proximity factors,  $\langle P \rangle_{mean}$ , will be compared among the levels:

- The sequence check begins with the first burst. If this burst contains less than three levels, it will be skipped and the next bursts is loaded, until the actual burst has more than 3 levels. The first level of this burst is loaded.
- The successive two levels of the current level are loaded. The following proximity factor differences,  $dP_i$ , for the triple set of levels will be calculated:  $dP_1 = \langle P_2 \rangle - \langle P_1 \rangle$ ;  $dP_2 = \langle P_3 \rangle - \langle P_2 \rangle$ ; and  $dP_3 = \langle P_1 \rangle - \langle P_3 \rangle$ .
- The enzyme is moving in hydrolysis direction (in the order L→M→H, found in previous ATP hydrolysis experiments<sup>16</sup>), when two of the three  $dP_i$ -Values are greater than minimum difference of mean proximity factors,  $dP_{min}$ , and one is lower than 2 times of the difference  $-dP_{min}$ . Only those triples of levels will be accepted that agree to this condition.
- Level number two will be loaded and step 2 and 3 will be processed again, until the last three levels of the burst are checked.

However, to prove the reliability of the automatic burst analysis, we manually analyzed the time resolved single-molecule FRET data sets in parallel.

## RESULTS

### 3.1. Distinct FRET efficiencies in the presence of AMPPNP

ATP synthesis and ATP hydrolysis are accomplished by intramolecular rotation of the subunits  $\gamma\epsilon_{10}$  in  $F_0F_1$ -ATP synthase. Adding an ATP derivative like AMPPNP, which binds to one of the three catalytic binding sites but cannot be hydrolyzed, stops the rotation. Accordingly, the enzyme is trapped in one of three orientations of the  $\gamma\epsilon_{10}$ -rotor assembly. In the presence of AMPPNP, fixed orientations of the  $\gamma$ - and the  $\epsilon$ -subunit in  $F_0F_1$ -ATP synthase have been observed in the previous single-molecule FRET experiments<sup>11,12</sup> using a rhodamine dye as the FRET donor at the rotating subunit and Cy5 as the FRET acceptor bound to the  $b$ -subunit dimer.

As an alternative to the chemical attachment of fluorophores, we evaluated the possibility to fuse genetically an autofluorescent protein, EGFP, to the  $a$ -subunit of ATP synthase. If protein folding is not perturbed by the short linker between the EGFP and the subunit of the enzyme, we can expect a labeling degree of 100%. We chose Alexa-568-maleimide as the FRET acceptor, because a high fluorescence quantum yield for the rhodamine had been reported<sup>17</sup> and a large spectral overlap between EGFP and Alexa-568 was expected resulting in a Förster radius of 5.3 nm according to the supplier (Molecular Probes, Eugene, OR, USA).

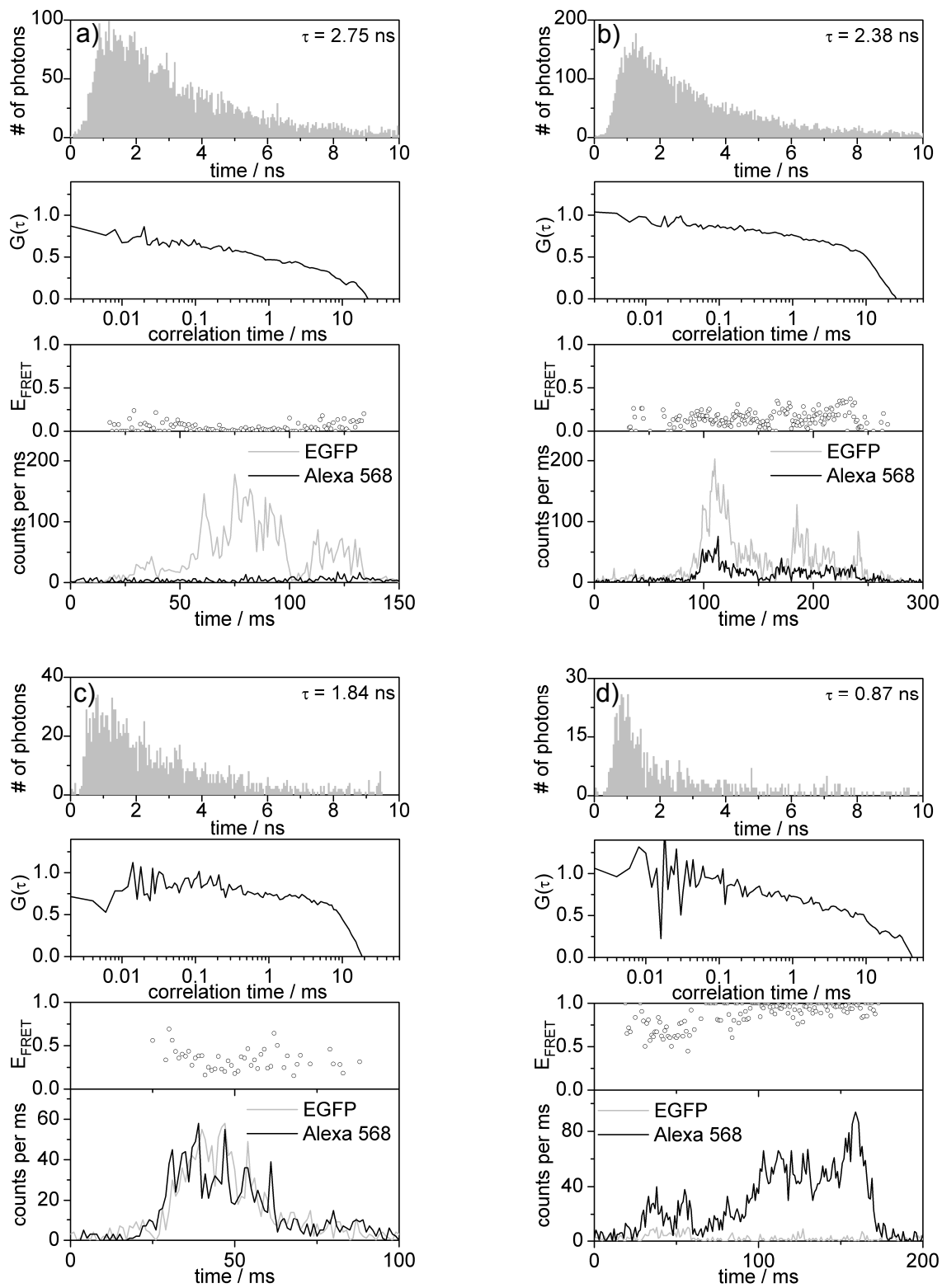


**Figure 1.** Photon bursts of four  $F_0F_1$ -ATP synthases in the presence of AMPPNP. Each burst is characterized by EGFP lifetime (upper panels), autocorrelation function for EGFP photons (middle panels), FRET efficiency traces (dots) and corrected fluorescence intensities traces with 1 ms time binning (gray lines for donor, black lines for acceptor channel).

Two independent mutants of F<sub>o</sub>F<sub>1</sub>-ATP synthases from *Escherichia coli* were required: one contained the EGFP fusion to the C-terminus of the  $\alpha$ -subunit in the F<sub>o</sub> part, the second was the cysteine mutant in the  $\epsilon$ -subunit of the F<sub>1</sub> part. The cysteine was introduced as residue 56 in the  $\epsilon$ -subunit at a position which is located on the surface of the subunit and is exposed to the buffer<sup>11</sup>. At first, the F<sub>o</sub> parts with the EGFP were isolated and reconstituted in liposomes. Secondly, we prepared the F<sub>1</sub> parts, labeled the  $\epsilon$ -subunit, and, in the presence of Mg<sup>2+</sup>, both parts were reassembled to yield the fully functional FRET-labeled ATP synthases with not more than one enzyme per lipid vesicle.

This FRET-labeled ATP synthases in liposomes were diluted to obtain a EGFP-F<sub>o</sub>F<sub>1</sub> concentration of approximately 100 pM. We observed 1 to 3 single ATP synthases traversing one-by-one the detection volume of the confocal microscope within 5 s and, therefore, well-separated photon bursts in time. In this buffer, 1 mM AMPPNP was present to block rotation of the subunits  $\gamma\epsilon\alpha_{10}$ . Four different FRET efficiencies were found in these bursts as shown in Fig. 1. Most ATP synthases appeared to have no FRET acceptor. They were allocated to the 'donor only' fraction and were characterized by high photon count rates in the donor detection channel and nearly no counts in the acceptor channel. The mean fluorescence lifetimes of these EGFP-F<sub>o</sub>F<sub>1</sub> was  $\tau_D = 2.8$  ns (upper panel in Fig. 1 a). An apparent FRET efficiency was calculated using the background-corrected fluorescence intensities and the detection efficiencies for the two channels of our setup. As expected for a missing FRET acceptor, this apparent FRET efficiency was centered around 0.

The double-labeled ATP synthases in liposomes showed relatively higher count rates in the acceptor channel. The lifetimes of the single FRET donor was shorter than the 2.8 ns found for the 'donor only' ATP synthase. The lifetimes corresponded to three distinct ratios of donor intensity,  $I_D$ , and acceptor intensity,  $I_A$ . We attributed the FRET efficiencies to 'low FRET efficiency' (or L-state) with  $E_{FRET}$  ranging from 0.1 to 0.4, 'medium FRET efficiency' (M-state) for  $E_{FRET}$  from 0.4 to 0.7, and 'high FRET efficiency' (H-state) for  $E_{FRET}$  from 0.7 to 1. For all bursts we calculated the donor intensity autocorrelation function to identify those liposomes with more than one single ATP synthase. From this AMPPNP experiment, we concluded that we were able to discriminate the three stopping positions of the  $\epsilon$ -subunit with respect to the  $\alpha$ -subunit by their FRET efficiency.

### 3.2. Fluctuating FRET efficiencies in the presence of ATP

We changed the buffer and added 1 mM ATP instead to start the ATP hydrolysis reaction. The FRET-labeled single ATP synthases showed fluctuations of the FRET efficiencies within a single photon burst (Fig. 2 a,b) indicating rotation of the  $\epsilon$ -subunit during catalysis. Depending on the observation time of the freely diffusing enzyme, we observed three and more distinct FRET efficiency levels with stepwise changes. The dwell times, that is, the duration of these FRET levels, were found in the range of several ms to hundreds of ms. However, the data set was not large enough for a statistical analysis of the dwell times and a comparison with biochemical turnover numbers per enzyme<sup>11,12</sup>.

The distance between the donor and the acceptor fluorophore,  $r_{DA}$ , results from the conversion of the intensity values into nanometer distances according to the Förster theory of resonance energy transfer<sup>9,10</sup>:

$$r_{DA} = R_0 \cdot ((E_{FRET})^{-1} - 1)^{1/6} \quad (1)$$

with the intensity-defined FRET efficiency

$$E_{FRET} = I_A / (I_A + \gamma I_D) \quad (2)$$

(with  $\gamma = \eta_A \phi_A / \eta_D \phi_D$  using the detection efficiencies of the set-up for acceptor and donor,  $\eta$ , and the quantum yields,  $\phi$ ) or based on the donor fluorescence lifetimes,  $\tau_{DA}$ , in the presence of the FRET acceptor (or  $\tau_D$  in the absence, resp.)

$$E_{FRET} = 1 - (\tau_{DA} / \tau_D) \quad (3)$$

The ATP synthase in Fig 2 a switched from the L-level with  $E_{FRET}=0.16$  and  $\tau_{DA}=2.22$  ns after 90 ms observation time to the M-level ( $E_{FRET}=0.42$ ;  $\tau_{DA}=1.87$  ns), and after 130 ms to the H-level ( $E_{FRET}=0.87$ ;  $\tau_{DA}=0.56$  ns). The second ATP synthase switched from the L-level with  $E_{FRET}=0.24$ ;  $\tau_{DA}=2.27$  ns) via the M-level ( $E_{FRET}=0.36$ ;  $\tau_{DA}=1.71$  ns) to the H-level ( $E_{FRET}=0.87$ ;  $\tau_{DA}=0.56$  ns) in Fig. 2 b.

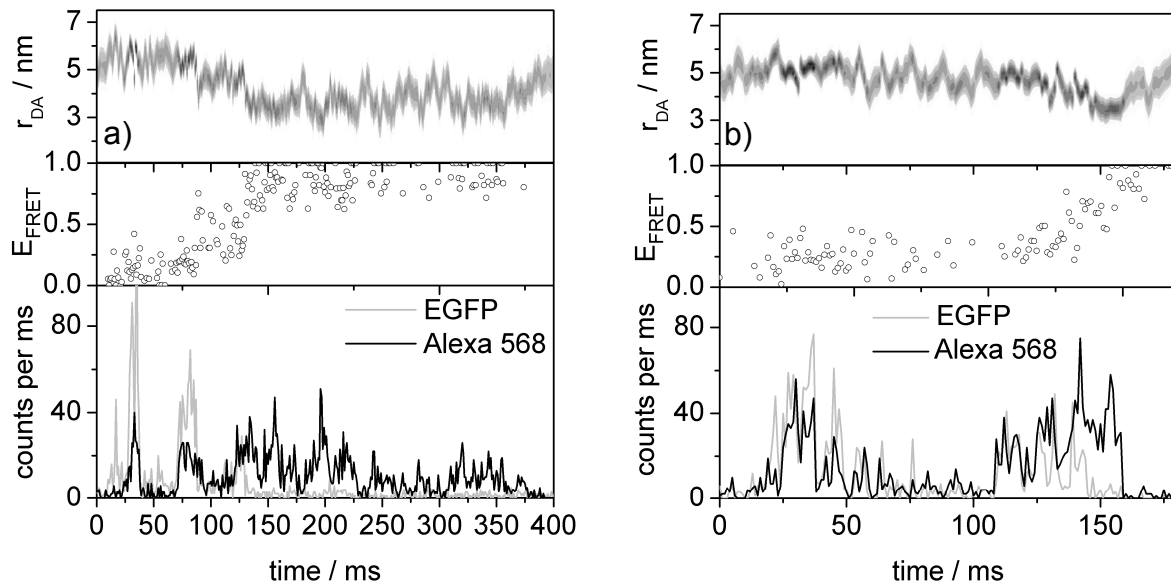


**Figure 2.** Conformational changes in two  $F_0F_1$ -ATP synthases in the presence of ATP. Lower panels, fluorescence intensity trajectories (EGFP: gray lines; Alexa-568: black lines) with 1 ms binning. Middle panels, corresponding FRET efficiencies. Upper panels, distance trajectories between both fluorophores calculated with 'FRET TRACE'<sup>18</sup>.

A straight forward way to analyze the distance changes in the ATP synthase during catalysis would be by the calculation of a distance trajectory for  $r_{DA}$  between the EGFP at the  $\alpha$ -subunit and the Alexa-568 at the rotating  $\varepsilon$ -subunit. However, the small number of recorded photons per time bin leads to large errors for a distance trajectory calculated from each data point. Therefore, we used a novel analysis method which is based on single photons detected with the high time resolution provided by the TCSPC data. Following G. Schröder and H. Grubmüller, the time trajectory of the distance between the two FRET fluorophores,  $r_{DA}$ , can be described by a one dimensional random walk with a transition probability of the distance from one time bin to the next<sup>18</sup>. Calculated with the free software package 'FRET TRACE', this method yields auxiliary information of the uncertainty of the calculated distances, and, furthermore, considers the whole information of the photon arrival times. It is therefore independent of pre-defined time bins that were used to visualize the photon burst in the intensity trajectories (lower panels in Fig. 2).

The probabilities of distance changes (or rotary steps in the case of ATP synthase, respectively) depend on an unknown so-called 'effective diffusion parameter  $D$ ' that describes the kinetics of the conformational changes. From cross-validation of several models with different effective diffusion coefficients, we obtained an effective diffusion coefficient of  $D=2.0 \cdot 10^{-16} \text{ m}^2/\text{s}$  for our FRET data. The second necessary assumption is the Förster radius  $R_0$  as derived from the spectral overlap and the quantum yields. Here, we used the smaller value  $R_0=4.88 \text{ nm}$  for the EGFP-Alexa-568 pair (see below). As shown in the upper panels of Fig 2, the distance changes in the presence of ATP calculated with 'FRET TRACE' occurred stepwise and at the same time as seen in the FRET efficiency trajectory. At low photon count rates within the burst, the fluctuations of the FRET efficiency trajectory for one particular level were too large to identify conformational changes, but in the distance trajectories the FRET level transitions could still be observed. However, as the time resolution is still related to the photon count rates, higher detection efficiencies for the single FRET-labeled ATP synthases have to be achieved.

### 3.3. Three distances of position $\varepsilon 56$ with respect to the $\alpha$ -subunit during ATP hydrolysis

The FRET level analysis with 'FRET TRACE' supported the three levels in selected single photon burst with stepwise interchanging levels. To get an overview of the different FRET levels and the number of rotating ATP synthases in our

measurements, we plotted all photon burst of this data set in two-dimensional histogram of donor lifetime  $\tau_{DA}$  versus the intensity ratio  $I_D/I_A$ . Rewriting equation (2) yields

$$(I_D/I_A) = ((E_{FRET})^{-1} - I) \cdot \gamma^{-1} = (\tau_{DA} / (\tau_D - \tau_{DA})) \cdot \gamma^{-1} \quad (4)$$

Combining equations (1) and (3) results in

$$r_{DA} = R_0 \cdot (\tau_{DA} / (\tau_D - \tau_{DA}))^{1/6} \quad (5)$$

Thereby, other photophysical effects like donor or acceptor quenching are easily identified in the 2D plot<sup>19</sup>.

We compared two different ways of burst and FRET level identification: the manual selection method of individual photon bursts (which is a time demanding process) and a threshold-based software approach for future automatic filtering and fast processing of large FRET data sets. As shown in Fig. 3 a, the manually selected histogram consists of 3782 bursts with 4536 FRET levels. Photon bursts with 1, 2, 3, and more FRET level were combined in the 2D plot. The automatic level detection of the same data set is shown in Fig. 3 b and resulted in a similar 2D distribution from 2971 photon bursts with 3580 FRET levels. Most FRET efficiencies were characterized by a donor lifetime around 2.5 ns and  $\log(I_D/I_A) = 1.2$ , and were identified as the 'donor only' population, that is, F<sub>0</sub>F<sub>1</sub>-ATP synthases without Alexa-568 at the  $\varepsilon$ -subunit. Another large fraction of molecules were found to be located in the 'high FRET level' area of the 2D plot with a donor lifetime of 0.4 ns and a  $\log(I_D/I_A) = -1.1$ . These FRET levels originated from bursts with only one FRET state, and, as the number of donor photons to calculate the lifetime was very low, the maximum likelihood estimation of these lifetimes exhibited a larger error.

From both data sets we created the sub-sets of those photon bursts, which comprised three and more FRET levels and ensured a rotation of the  $\varepsilon$ -subunit. The additional requirement of the right level sequence  $\rightarrow L \rightarrow M \rightarrow H \rightarrow$  as expected for ATP hydrolysis reduced the number of manually selected levels to 393. Furthermore, an intensity threshold was used to remove the bursts consisting of a 'donor only level' as the last level in the burst. We wanted to filter out those photophysical events of acceptor bleaching which would be interpreted as an apparent FRET efficiency transition or a rotary step of subunit  $\varepsilon$ . A total of 307 FRET level from 92 bursts remained in Fig. 3c. Applying the same criteria yielded 96 remaining FRET levels from 24 bursts after the automatic level detection process (Fig. 3 d).

We defined three areas in the 2D plots to classify the FRET levels. The low-FRET efficiency levels were located within the lifetime limits of  $2.2 \text{ ns} < \tau_{DA} (L) < 2.8 \text{ ns}$  and the intensity ratio range  $-0.2 < \log(I_D/I_A) < 0.9$ . The medium-FRET efficiency levels were located within the lifetime limits of  $1.3 \text{ ns} < \tau_{DA} (M) < 2.2 \text{ ns}$  and the intensity ratio range  $-0.5 < \log(I_D/I_A) < 0.2$ , and the high-FRET efficiency levels were located within the lifetime limits of  $0.4 \text{ ns} < \tau_{DA} (H) < 1.3 \text{ ns}$  and the intensity ratio range  $-1.0 < \log(I_D/I_A) < -0.4$ . This resulted in 98 L-levels, 72 M-levels and 42 H-levels in Fig. 3 c, and in 26 L-levels, 30 M-levels and 40 H-levels in Fig. 3 d. The mean lifetimes and the associated mean  $\log(I_D/I_A)$  values were calculated for each of the three populations to yield three stopping positions of the  $\varepsilon$ -subunit during ATP hydrolysis. Accordingly, the L-level had a mean lifetime  $\tau_{DA} (L) = 2.489 \text{ ns}$  and a mean  $\log(I_D/I_A) = 0.349$  in the manually selected FRET levels, the M-level had a mean lifetime  $\tau_{DA} (M) = 1.764 \text{ ns}$  and a mean  $\log(I_D/I_A) = -0.06$ , and the H-level had a mean lifetime  $\tau_{DA} (L) = 0.887 \text{ ns}$  and a mean  $\log(I_D/I_A) = -0.734$ . For the software-analyzed FRET levels, a mean lifetime  $\tau_{DA} (L) = 2.506 \text{ ns}$  and a mean  $\log(I_D/I_A) = 0.338$  was found for the L-level, a mean lifetime  $\tau_{DA} (M) = 1.768 \text{ ns}$  and a mean  $\log(I_D/I_A) = -0.102$  was found for the M-level, and a mean lifetime  $\tau_{DA} (H) = 0.899$  and a mean  $\log(I_D/I_A) = -0.694$  was found for the H-level. Considering the low number of the remaining FRET levels used for the calculation of the mean values, the agreement of both the manual burst-by-burst method and the automatic threshold-based method is excellent.

Both triple sets of mean L-, M- and H-level were located near the black straight lines in the 2D plots, which indicates nearly perfect FRET behavior and not quenching<sup>19</sup>. However, the black line represents FRET for a specific ratio of about 2 for the quantum yields of Alexa-568 and of EGFP. This ratio could be most likely realized assuming a lower quantum yield of 0.35 for EGFP fused to the  $\alpha$ -subunit at our excitation conditions (instead of 0.6 as reported), and of 0.67 for Alexa-568 (that is the highest quantum yield reported for this fluorophore bound to a protein<sup>17</sup>).

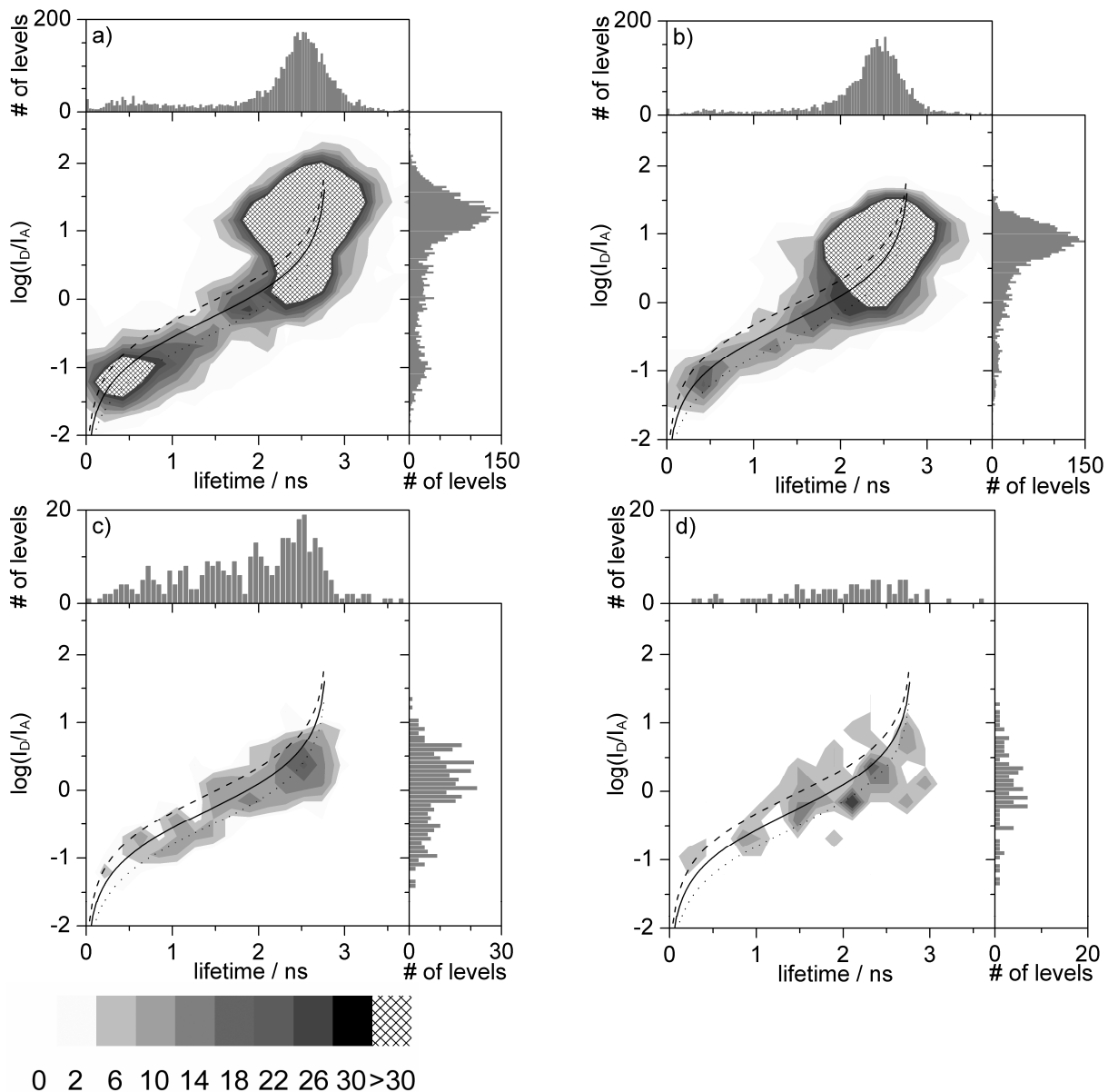


**Figure 3.** Manually selected (left side) and automatically detected (right side) FRET levels in single ATP synthases in the presence of 1 mM ATP. **a**, all FRET levels of photon bursts exceeding 20 counts/ms for EGFP or 10 counts/ms for Alexa-568. In total, 3782 bursts were selected, 3391 with one state, 187 with two, and 404 with three and more FRET levels within one burst. **b**, all automatically detected FRET levels according to the thresholds used in (a). In total, 2971 bursts were detected, 2598 with one state, 228 with two, and 145 with three and more FRET levels. **c**, sub-set of (a) by selecting bursts with three or more levels, with the level sequence of low–medium–high FRET, and with a minimum of 40 photons in the donor channel per level. If the mean average count rate in the donor channel was less than 25 counts/ms then the logarithmic ratio  $\log(I_D/I_A)$  had to be smaller than 0.4. Thereby, 92 ATP synthase remained. **d**, sub-set of the automatically found bursts selected in the same fashion as in (c), consisting of 24 remaining ATP synthases. The gray scale bar indicates the frequency of levels in (a) and (b). In (c) and (d), the gray scales were adjusted to match each maximum frequency.

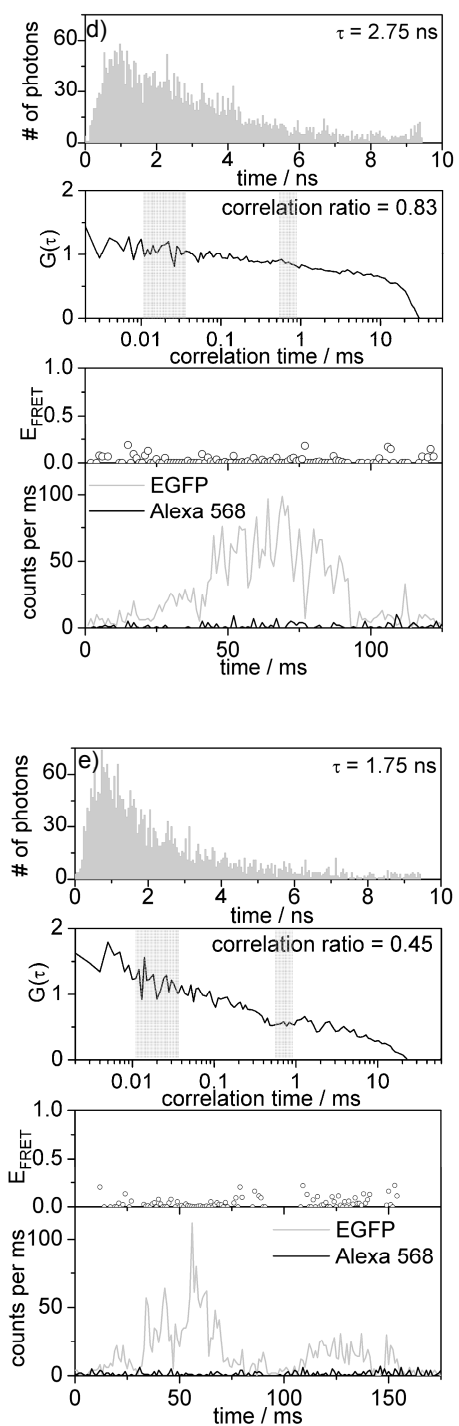
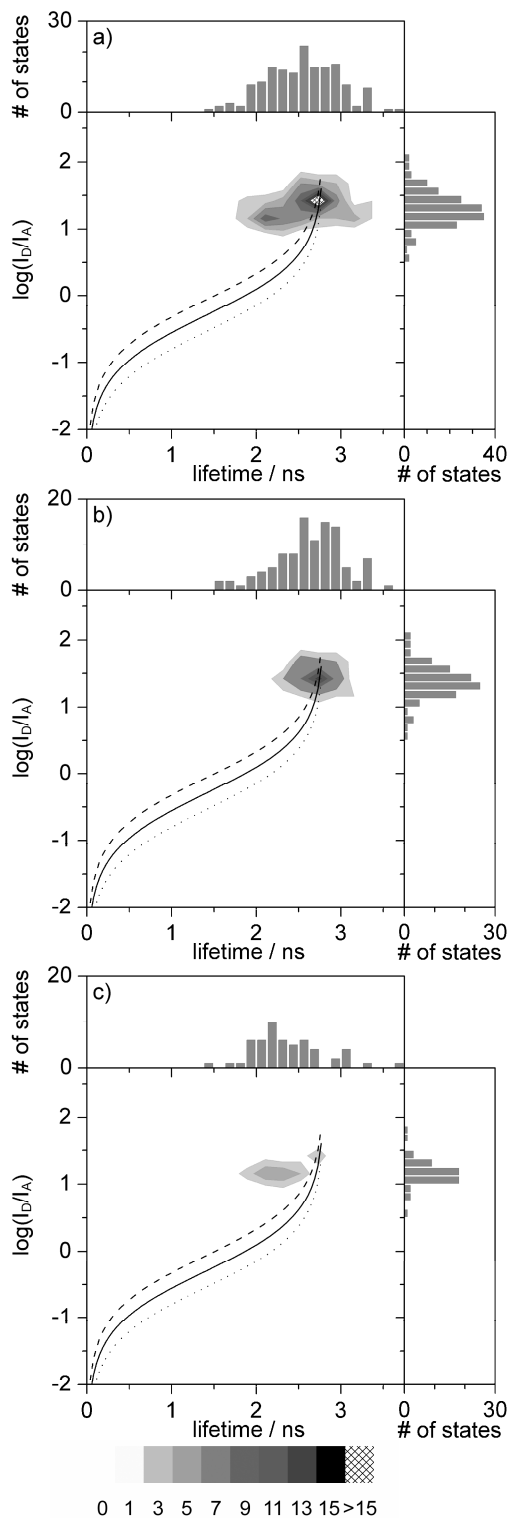


**Figure 4.** 'Donor only' bursts of EGFP-F<sub>0</sub>F<sub>1</sub>-ATP synthases in buffer at pH 8.0. **a**, all bursts. **b**, subensemble I selected by a minimum average count rate  $\langle I_{min} \rangle > 15$  counts/ms; **c**, subensemble II selected by  $\langle I_{min} \rangle < 15$  counts/ms. Gray scale indicates frequency of states. **d**, photon burst of subensemble I, with lifetime, autocorrelation function, and two-channel intensity trajectory. **e**, photon burst of subensemble II of EGFP-F<sub>0</sub>F<sub>1</sub>-ATP synthase.

### 3.4. Identification of two different EGFP-F<sub>0</sub>F<sub>1</sub> populations

We noticed a high number of FRET states in 2D plots of all FRET levels during ATP hydrolysis, that exhibited a lifetime similar to the low-FRET level but a too high ratio of donor-acceptor intensities compared to the bursts that were selected for rotation. These photon bursts with the shortened lifetimes are far off the limited area defined by the theoretical lifetime-versus- $\log(I_D/I_A)$  dependencies shown as the black dashed and dotted lines in the 2D plots in Fig. 3. At next, we aimed at the identification of this short-lifetime, red-shifted and dark 'donor-only' population. Therefore, we measured the 'donor-only' fraction independently using the same two spectral ranges for EGFP fluorescence detection. The EGFP was fused to the  $\alpha$ -subunit of F<sub>0</sub>F<sub>1</sub>-ATP synthase in liposomes but an intramolecular acceptor fluorophore was absent in the enzyme. The data set consisted of a small number of 161 molecules but revealed two populations: subensemble I was centered around a lifetime of 2.8 ns with  $\log(I_D/I_A) = 1.4$ , and the second population, subensemble II, had a lifetime of about 2.0 ns with  $\log(I_D/I_A) = 1.2$  (Fig. 4 a). In previous ensemble lifetime measurements of EGFP-F<sub>0</sub>F<sub>1</sub>-ATP synthase in liposomes, we had measured a single lifetime component  $\tau = 2.77$  ns using a ns-pulsed diode for excitation around 460 nm (Fluotime 200, Picoquant, Germany).

The excited state of EGFP and others autofluorescent proteins has been investigated with high-resolution ensemble spectroscopy and single-molecule spectroscopy methods. It has been shown, that the chromophore in autofluorescent proteins is sensitive to the pH of the buffer resulting in a on-off flickering of the fluorescence in the microsecond time range<sup>20</sup>. This can be measured by fluorescence correlation spectroscopy. Therefore, we calculated the individual autocorrelation functions of each photon burst,  $G(\tau)$ . As shown in Fig 4 d, a bright burst of EGFP-F<sub>0</sub>F<sub>1</sub>-ATP synthase belonging to subensemble I (according to the lifetime  $\tau = 2.75$  ns) showed a constant  $G(\tau)$  of about 1 in for correlation times between 1  $\mu$ s and 1 ms. The correlation ratio of 0.83 for the mean  $G(\tau)$  values in the range of 500-700  $\mu$ s and the range of 10-40  $\mu$ s indicated that no flickering was observed in this burst. In contrast, an ATP synthase belonging to subensemble II (lifetime  $\tau = 1.75$  ns) showed a correlation ratio of 0.45, that is,  $G(\tau)$  dropped in the 500-700  $\mu$ s range due to fast on-off flickering of the fluorescence. We found a mean value for the correlation ratio in this data set of about 0.66. However, it was not possible to clearly separate the two subensembles I and II using arbitrary thresholds for the calculated correlation ratio, because the correlation ratio values were equally distributed for all lifetimes between 1.7 ns and 3.0 ns.

Using a mean minimum intensity,  $\langle I_{min} \rangle$ , of 15 counts per ms in the spectral range from 498-567 nm ('donor channel') as the threshold enabled us to separate both subensembles. For  $I_{min} > 15$  counts/ms, the subensemble I consisted of 103 molecules (Fig. 4 b). Accordingly, the subensemble II with the shorter lifetime has a red-shifted fluorescence emission and, with  $I_{min} < 15$  counts/ms, seems to have a lower quantum yield. In Fig 4 c, 53 molecules constituted subensemble II.

### 3.5. Triangulation of the EGFP at the $\alpha$ -subunit

The goal of this work was to evaluate the possibilities of a three-dimensional localization of the  $\alpha$ -subunit in the F<sub>0</sub> part of ATP synthase using pulsed excitation for single-molecule FRET distance measurements. From the FRET data of Fig 3 c and d, we could calculate a triple set of distances between the fluorophores at the  $\alpha$ -subunit and the  $\epsilon$ -subunit according to equations (1) or (5), respectively. The most likely value for the Förster radius was  $R_0 = 4.88$  nm using the quantum yields of 0.35 for EGFP fused to the  $\alpha$ -subunit and of 0.67 for Alexa-568 bound to the cysteine at position 56 of the  $\epsilon$ -subunit. During ATP hydrolysis, the L-level distance  $d(L) = 6.90$  nm was calculated from the lifetime-based  $E_{FRET} = 0.11$ , the M-level distance  $d(M) = 5.33$  nm was calculated from  $E_{FRET} = 0.37$ , and the H-level distance  $d(H) = 4.27$  nm was calculated from  $E_{FRET} = 0.69$ . These distances were used for a triangulation of the EGFP position at the C-terminus of the  $\alpha$ -subunit.

Furthermore, the two assumptions were needed to develop the 3D model as depicted in Fig 5.

- The three stopping position of  $\epsilon 56$  are separated by 120° rotation steps around an axis of rotation, which is placed along the middle of the  $\gamma$ -subunit, and
- the stopping positions of the rotating  $\epsilon 56$  residue are located on a ring with a radius of 2.5 nm, that is, the off-axis distance from the axis of rotation in F<sub>0</sub>F<sub>1</sub>-ATP synthase.

This radius was chosen to match the size of the rotating  $c$ -ring in the  $F_0$  part of ATP synthase which was determined by X-ray crystallography<sup>7</sup>. These boundary conditions combined with the FRET level sequence  $\rightarrow L \rightarrow M \rightarrow H \rightarrow$  for the rotation direction during ATP hydrolysis resulted in two positions of the EGFP with respect to the  $\epsilon 56$  positions, that are mathematically equivalent. The triangulation principle is shown in Fig 5 a. The three black balls represent the  $\epsilon 56$  positions, the silver balls the resulting two symmetric positions of EGFP. In the model of the  $F_0F_1$ -ATP synthase, the Alexa-568 is located at the three stopping positions indicated by the black balls. However, if we use the position  $b64$  (light gray ball in Fig. 5 b and c) as the reference to the  $b$ -subunit dimer and place the  $a$ -subunit adjacent to the  $b$ -dimer, still two orientations of the  $a$ -subunit have to be distinguished: one position is located to the left hand side (Fig. 5 b), the other is found on the right hand side (Fig. 5 c). To make a decision between these sides, an additional information is needed.

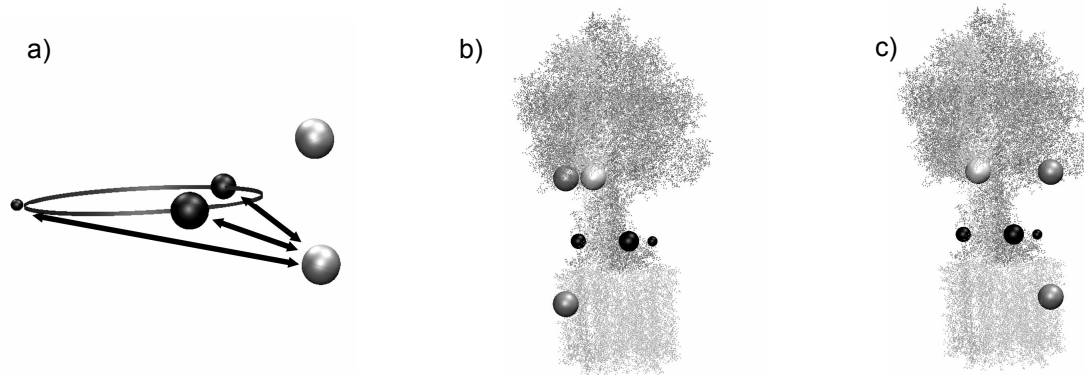


**Figure 5:** Triangulation of the  $a$ -subunit in a model of *E. coli* ATP synthase with three stopping positions of  $\epsilon 56$  (black balls), the position of  $b64$  (light gray ball) according to previous single-molecule FRET triangulations<sup>11,21,22</sup>, and the two mathematically equivalent positions of EGFP (silver balls) at the height of  $b64$  (upper positions) or at the lipid membrane level (lower positions). Two possible orientations for EGFP, which are shifted by  $120^\circ$  along the axis of rotation in  $F_0F_1$ , on each side of the  $b$ -subunit dimer have to be discussed (see text).

The previous single-molecule FRET experiments with one fluorophore at the rotating  $\epsilon$ -subunit and the second one at the non-rotating  $b$ -subunits unraveled the asymmetry for the three stopping positions of  $\epsilon 56$ <sup>11</sup>. The three dwell times were slightly different and the populations of the three FRET states in the presence of AMPPNP and in buffer without nucleotide were non-equally distributed. For AMPPNP, most enzymes were found in the H-state; but for buffer conditions, more than 50 percent of the ATP synthases were resting in the L-state. Because our actual FRET data set is too small for allow for the assignment according to the dwell times, we analyzed the populations for the two biochemical conditions. The 2D plots are shown in Fig. 6. In the presence of AMPPNP, 4092 FRET states were found in total (Fig. 6a), most of them 'donor only' ATP synthase. In buffer, 3888 enzymes were found and, again, approximately 70 percent were 'donor only' ATP synthases. These 'donor only' population with the two subensembles I and II could be decreased using two thresholds. Following the criteria for the level attribution in the case of ATP hydrolysis, three areas in the 2D plots were defined for the L-, M- and H-states and the remaining ATP synthases were counted for each FRET states. Because the number of molecules in the L-state orientation is obscured by the threshold process to remove the 'donor only' fraction, we concentrated in the relative amounts of H-states and M-states. For AMPPNP, we found 98 H-states and 107 M-state. In buffer, 95 H-states and 182 M-states were counted. Compared to Fig. 6 a and b, it became obvious that the number of remaining H-states was affected by the thresholds used for Fig c and d. Accordingly, we could only state that in the absence of ATP or AMPPNP the relative number of M-states compared to the H-states is higher than in the presence of AMPPNP. Placing the positions of EGFP to the right hand side of the  $b$ -subunit dimer would match the expectations from the previous experiments of  $\epsilon$ -subunit rotation. Therefore, we prefer the positioning of the  $a$ -subunit as shown in Fig 5 c.

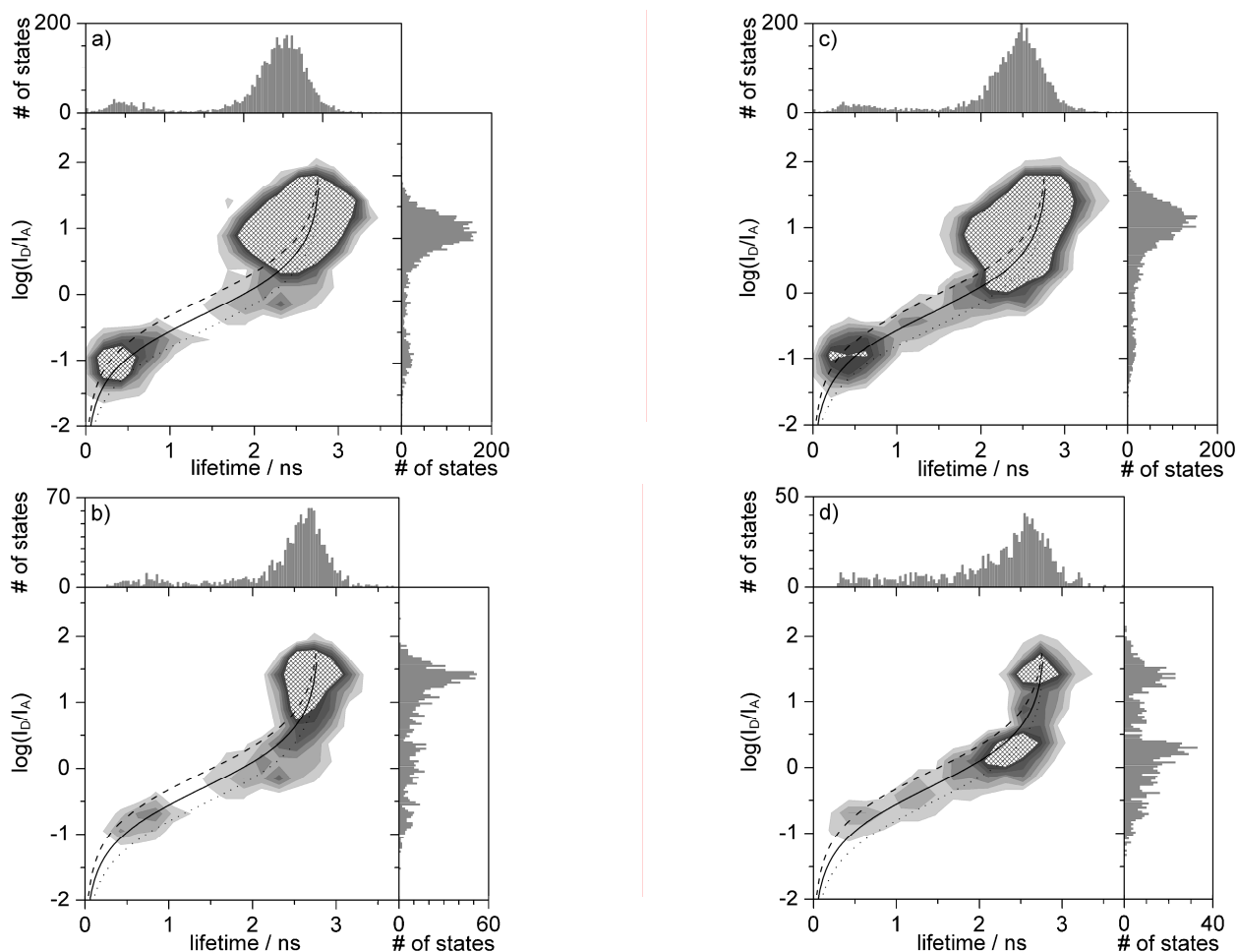


**Figure 6.** FRET states of single ATP synthases in the presence of 1mM AMPPNP (left side) and in buffer without AMPPNP (right side). **a**, all bursts with minimum photon counts  $I_{min} > 150$  in the donor channel. **b**, sub-set of (a) selected by  $\log(I_D/I_A) < 0.4$  if the average count rate on the donor channel was smaller than 25 counts per ms. **c**, All bursts with  $I_{min} > 150$ . **d**, sub-set of (c) selected by  $\log(I_D/I_A) < 0.4$  if the average count rate  $\langle I_{min} \rangle$  was  $< 25$  counts/ms.

## DISCUSSION

We have presented the first time resolved single-molecule FRET data to triangulate the position of the  $\alpha$ -subunit of the  $F_0F_1$ -ATP synthase from *E. coli*. Therefore, EGFP was fused to the C-terminus of this subunit to serve as the FRET donor fluorophore. As the FRET acceptor, Alexa-568 was attached to the rotating  $\varepsilon$ -subunit. The enzymes had been embedded into the membrane of lipid vesicles (approximately 100 nm diameter) to yield not more than a single ATP synthase per liposome. The freely diffusing enzymes were excited with ps pulses at 490 nm with a repetition rate of 80 MHz in a confocal microscope. The high time resolution needed to discriminate the lifetimes between 0.5 ns and 2.8 ns was achieved by the short ps pulses and the fast TCSPC electronics. Three biochemical conditions were applied: rotary catalysis during ATP hydrolysis, AMPPNP trapping of rotation, and resting in the buffer without nucleotides. These conditions enabled us to calculate a triple set of FRET distances for the triangulation, and to make a preliminary decision for the orientation of the  $\alpha$ -subunit with respect to the  $b$ -subunit dimer.

In contrast to cw excitation, using a pulsed laser allowed for the lifetime-based FRET efficiency measurements that avoid many of the difficulties calculating intensity-based FRET efficiencies: background correction, cross-talk

correction, determination of the detection efficiencies of the set-up for donor and acceptor channel, and, most importantly, the determination of the quantum yields for donor and acceptor fluorophore in the local protein environments. We noticed a strong dependence of the intensity ratio  $\log(I_D/I_A)$  and the distances between the two fluorophores calculated from the intensity-based FRET efficiencies. Within the 2D histograms created from intensities and lifetimes of each FRET level, we could identify and remove those photon bursts with non-FRET behavior. For the first time we identified a subensemble of the EGFP-F<sub>0</sub>F<sub>1</sub> with distinct photophysics, that was not noticed in earlier cw-excited single-molecule FRET experiments with this ATP synthase. Here, a set of thresholds could be used to remove this population. Furthermore, as lifetime and intensity ratio are related by  $E_{FRET}$ , the theoretical FRET curves assuming different quantum yields of donor and acceptor could be used to evaluate the published values and to estimate the corrections for the local protein environments. However, using direct excitation of Alexa-568 bound to F<sub>0</sub>F<sub>1</sub>-ATP synthase at 561 nm yielded similar photon count rates as for rhodamine B, and only half of the counts compared to a single TexasRed fluorophore. Accordingly, a quantum yield of 0.7 for Alexa-568 at  $\epsilon_{56}$  (as assumed from the FRET curves in the 2D histograms) seems to be too high, and this method should be used only to get an estimate for the quantum yields.

A disadvantage of pulsed excitation might be the high peak power. Especially for EGFP, photobleaching was a serious problem, because we had to apply a mean power of 200  $\mu$ W at 490 nm to detect a high number of photons from a single ATP synthase. The autofluorescent proteins are known to exhibit spectral fluctuations depending on the charge at the fluorophore. The fluorescent anionic B-state of the EGFP is the dominant conformation, the neutral A-state is not excited with 490 nm<sup>23</sup>. Recently, also red-shifted emission of single EGFP and EYFP has been reported<sup>24</sup>, and, induced by irradiation, the GFP could be converted to a red-fluorescent chromophore<sup>25</sup>. Using ps pulses in a power series from 50 to 500  $\mu$ W at 490 nm, we observed power-dependent lifetime changes of single EGFP-F<sub>0</sub>F<sub>1</sub>. At 500  $\mu$ W, the average lifetime of a single EGFP dropped to 2.2 ns. It might be possible, that the subensemble of EGFP with the shorter lifetime and red-shifted emission had been generated during our pulsed measurements, but further investigations are required to identify the details of the photophysics of EGFP fused to the  $\alpha$ -subunit of F<sub>0</sub>F<sub>1</sub>-ATP synthase.

Progress has been made towards an automatic threshold-based FRET analysis of photon bursts using the software 'Burst Analyzer'. Direct comparison of manually selected and automatically detected FRET levels during ATP hydrolysis revealed nearly perfect matching. However, the automatic detection did find not all positive events, or, vice versa, was not biased by the very low number of remaining FRET levels. Implementation of the lifetime calculation of the selected bursts or FRET levels, and of the different autocorrelation functions to estimate the number of fluorescent emitters in a single burst provide the basis for a detailed subensemble analysis and the discrimination of FRET processes from quenching. Furthermore, generating dynamic distance trajectories with 'FRET TRACE' is an alternative to the static FRET level distance calculations. With these features we can now start the FRET experiments on  $c$ -ring rotation, the proton-driven F<sub>0</sub> motor of ATP synthase. Achieving higher detection efficiencies for the single fluorophores with novel detection schemes will enable us to improve the time resolution and the precision of conformational change measurements by our single-molecule FRET approach to monitor catalysis in real time.

### Acknowledgements

The authors want to thank Prof. Dr. P. Gräber (University of Freiburg, Germany) and Prof. Dr. J. Wrachtrup (University of Stuttgart, Germany) for their support of the single-molecule studies with F<sub>0</sub>F<sub>1</sub>-ATP synthase. Financial support from the Landesstiftung Baden-Württemberg for 'functional nanodevices', the Deutsche Forschungsgemeinschaft (BO 1891 / 8-1), and the Graduiertenkolleg 'Biochemie der Enzyme', University of Freiburg, is gratefully acknowledged.

## 5. REFERENCES

1. M. Yoshida, E. Muneyuki, T. Hisabori, "ATP synthase - a marvellous rotary engine of the cell", *Nat. Rev. Mol. Cell Biol.*, **2**, 669-677, 2001.
2. R. A. Capaldi, R. Aggeler, "Mechanism of the F<sub>1</sub>F<sub>0</sub>-type ATP synthase, a biological rotary motor", *Trends Biochem. Sci.*, **27**, 154-160, 2002.
3. J. Weber, A. E. Senior, "ATP synthesis driven by proton transport in F<sub>1</sub>F<sub>0</sub>-ATP synthase", *FEBS Lett.*, **545**, 61-70, 2003.
4. B. Böttcher, I. Bertsche, R. Reuter, P. Gräber "Direct visualisation of conformational changes in EF<sub>0</sub>F<sub>1</sub> by electron microscopy", *J. Mol. Biol.*, **296**, 449-457, 2000.

5. J. L. Rubinstein, J. E. Walker, R. Henderson, "Structure of the mitochondrial ATP synthase by electron cryomicroscopy", *EMBO J.*, **22**, 6182-6192, 2003.
6. J. P. Abrahams, A. G. W. Leslie, R. Lutter, J. E. Walker, "Structure at 2.8 Å resolution of F<sub>1</sub>-ATPase from bovine heart mitochondria", *Nature* **370**, 621-628, 1994.
7. T. Meier, P. Polzer, K. Diederichs, W. Welte, P. Dimroth, "Structure of the rotor ring of F-type Na<sup>+</sup>-ATPase from *Ilyobacter tartaricus*", *Science*, **308**, 659-662, 2005.
8. R. A. Fillingame, C. M. Angevine, O. Y. Dmitriev, "Coupling proton movements to c-ring rotation in F<sub>1</sub>F<sub>0</sub> ATP synthase: aqueous access channels and helix rotations at the a-c interface", *Biochim. Biophys. Acta*, **1555**, 29-36, 2002.
9. B. W. van der Meer, G. Cooker, S. S.-Y. Chen, "Resonance Energy Transfer: Theory and Data", VCH, New York, 1994.
10. T. Förster, "Zwischenmolekulare Energiewanderung und Fluoreszenz", *Ann. Phys.*, **2**, 55-70, 1948.
11. B. Zimmermann, M. Diez, N. Zarrabi, P. Gräber, M. Börsch, "Movements of the ε-subunit during catalysis and activation in single membrane-bound H<sup>+</sup>-ATP synthase", *EMBO J.*, **24**, 2053-2063, 2005.
12. M. Diez, B. Zimmermann, M. Börsch, M. König, E. Schweinberger, S. Steigmiller, R. Reuter, S. Felekyan, V. Kudryavtsev, C. A. M. Seidel, P. Gräber, "Proton-powered subunit rotation in single membrane-bound F<sub>0</sub>F<sub>1</sub>-ATP synthase", *Nat. Struct. Mol. Biol.*, **11**, 135-141, 2004.
13. T. Krebstakies, B. Zimmermann, P. Gräber, K. Altendorf, M. Börsch, J.-C. Greie, "Both rotor and stator subunits are necessary for efficient binding of F<sub>1</sub> to F<sub>0</sub> in functionally assembled *Escherichia coli* ATP synthase", *J. Biol. Chem.*, **280**, 33338-33345, 2005.
14. N. Zarrabi, B. Zimmermann, M. Diez, P. Gräber, J. Wrachtrup, M. Börsch, "Asymmetry of rotational catalysis of single membrane-bound F<sub>0</sub>F<sub>1</sub>-ATP synthase", *Proc. SPIE-Int. Soc. Opt. Eng.*, **5699**, 175-188, 2005.
15. J. Enderlein, R. Erdmann, "Fast fitting of multi-exponential decay curves", *Optics Comm.*, **134**, 371-378, 1997. Matlab-package "TCSPCfit": <http://www.joerg-enderlein.de/fluo/fluo.html>
16. M. G. Düser, Y. Bi, S. D. Dunn, M. Börsch, "The distance between the γ- and the a-subunit of the ATP synthase determined by single-molecule fluorescence resonance energy transfer", *Biochim. Biophys. Acta - Bioenergetics*, **1658**, 108 Suppl. S, 2004.
17. N. Panchuk-Voloshina, R. P. Haugland, J. Bishop-Stewart, M. K. Bhalgat, P. J. Millart, F. Mao, W. Y. Leung, R. P. Haugland, "Alexa dyes, a series of new fluorescent dyes that yield exceptionally bright, photostable conjugates", *J. Histochem. Cytochem.*, **47**, 1179-1188, 1999.
18. G. F. Schröder, H. Grubmüller, "Maximum likelihood trajectories from single molecule fluorescence resonance energy transfer experiments", *J. Chem. Phys.*, **119**, 9920-9924, 2003. Program "FRETtrace": <http://www.mpibpc.mpg.de/groups/grubmueller/start/software/frettrace/index.html>
19. M. Margittai, J. Widengren, E. Schweinberger, G. F. Schröder, S. Felekyan, E. Haustein, M. König, D. Fasshauer, H. Grubmüller, R. Jahn, C. A. M. Seidel, "Single-molecule fluorescence resonance energy transfer reveals a dynamic equilibrium between closed and open conformations of syntaxin 1", *Proc. Natl. Acad. Sci. USA*, **100**, 15516-15521, 2003.
20. U. Haupts, S. Maiti, P. Schwille, W. W. Webb, "Dynamics of fluorescence fluctuations in green fluorescent protein observed by fluorescence correlation spectroscopy", *Proc. Natl. Acad. Sci. USA*, **95**, 13573-13578, 1998.
21. G. F. Schröder, H. Grubmüller, "FRETsg: Biomolecular structure model building from multiple FRET experiments", *Comp. Phys. Comm.*, **158**, 150-157, 2004. Program "FRETsg": <http://www.mpibpc.mpg.de/groups/grubmueller/start/software/frets-g-1.0/frets-g.html>
22. W. Humphrey, A. Dalke, K. Schulten, "VMD visual molecular dynamics", *J. Molec. Graphics*, **14.1**, 33-38, 1996.
23. W. E. Moerner, "Single-molecule optical spectroscopy of autofluorescent proteins", *J. Chem. Phys.*, **117**, 10925-10936, 2002.
24. C. Blum, A. J. Meixner, V. Subramaniam, "Room temperature spectrally resolved single-molecule spectroscopy reveals spectral forms and photophysical versatility of *Aequorea* green fluorescent proteins", *Biophys. J.*, **87**, 4172-4179, 2004.
25. M. B. Elowitz, M. G. Surette, P.-E. Wolf, J. Stock, S. Leibler, "Photoactivation turns green fluorescent proteins red", *Curr. Biol.*, **7**, 909-912, 1997.